Briquetting of waste glass cullet fine particles for energy-saving glass manufacture

DENG, Wei, WRIGHT, Richard, BODEN-HOOK, Chris and BINGHAM, Paul <http://orcid.org/0000-0001-6017-0798>

Published version

DENG, Wei, WRIGHT, Richard, BODEN-HOOK, Chris and BINGHAM, Paul (2018). Briquetting of waste glass cullet fine particles for energy-saving glass manufacture. Glass Technology: European Journal of Glass Science and Technology Part A, 59 (3), 81-91.

Briquetting of waste glass cullet fine particles for energy-saving glass manufacture

Wei Deng [a], Richard Wright [b], Chris Boden-Hook [b] and Paul A Bingham [a,1]

[a.] Materials and Engineering Research Institute, Faculty of Arts, Computing, Engineering and Sciences, Sheffield Hallam University, City Campus, Howard Street, Sheffield S1 1WB, UK

[b.] Wright Engineering Ltd, Blyth Road, Worksop S81 8BP, UK

Abstract

Fine particles of glass cullet (fines) arising during glass recycling cannot presently be recycled into glass manufacture due to the potential for bubble formation and foaming. Consolidation of glass fines into briquettes could enable their re-introduction into furnaces, reducing waste and glass melting energies. Properties of briquetted cullet fines and briquette melting behaviour in soda-lime-silica glass batches are presented. Morphology and density of glass fines and briquettes; and briquette mass and mechanical properties as functions of time after formation were analyzed. Compressive strength increases linearly with time after briquette formation. With slight batch modifications to maintain the same final glass composition, up to 15 wt % briquettes were successfully added to a representative container glass batch and melted. Results confirm that briquette batch additions can provide equivalent final glass composition, optical absorption characteristics and redox to briquette-free batches, supporting their industrial uptake.

Keywords: glass; cullet; energy; emissions; briquette; consolidation

[1] Corresponding author, email p.a.bingham@shu.ac.uk

1. Introduction

It is well known that the introduction of recycled glass (cullet) into commercial industrial glass batches can significantly reduce glass melting energy requirements and CO_2 emissions.[1-3] Cullet can act as a fluxing agent and decreases the glass melting energy and thus Specific Energy Consumption (SEC). Compared to virgin (mined and man-made) glass batch raw materials, the melting energy consumption of cullet is approximately 70-75 % [4]. However, collection, recycling and transportation of cullet produces a significant fraction of fine particles which cannot be directly re-introduced into glass furnaces and are thus currently treated as a waste and discarded. The glass industry has strict requirements for the particle size distribution of batch components [5]. Specifically, very small particles (typically 6mm diameter or less and cannot be sorted using existing optical technology) of glass cullet or batch raw materials can cause dust formation prior to and after entry to the furnace [5]; entrainment of many tiny bubbles or "seed" in the glass melt; and foaming of the melt in furnace [6]. Moreover, fine particles can have both corrosive and erosive effects on furnace refractories [6, 7] and they can block or foul the checkers in furnace regenerators [7]. Typically 20% of recycled cullet is rejected on account of its fine particle size, and in the UK most of this is currently sent to landfill [8] or into aggregates. If the rejected cullet fines can be reclaimed or consolidated in such a way that they can be re-melted as glass batch constituents, the growing shortages of landfill sites and high-quality recycled cullet for glass manufacture could be alleviated, whilst at the same time replacing virgin (mined) raw materials, reducing batch CO_2

emissions, and reducing the SEC of glass manufacture (and therefore fuel CO_2 emissions as most glass furnaces are gas-fired).

In the present study a briquetting technology, utilizing a novel binder has been applied to the problem of glass cullet fines, with the aim of enabling their recycling and re-melting in industrial glass manufacture. The research described in this paper is the result of an ongoing project with the aim of gaining a clearer understanding of the effects of introducing briquetted glass fines into full-scale glass manufacture in terms of melting rates, refining, redox, colour and energy saving.

In addition to controlling the particle size distribution, granulation of virgin glass batch raw materials to avoid dust formation and evolution during melting has previously been attempted [9]. More widely, granulation (very small, < ca. 10 mm diameter), pelletisation (small, < ca. 20 mm diameter) and briquetting (larger, < ca. 50 mm diameter) processes have all been researched in the glass industry [9-11]. However, these methods have hitherto been applied only to virgin glass batch materials (i.e. sand, sodium carbonate, limestone, dolomite, etc.) and not to glass cullet fines [9, 11]. Different inorganic and organic chemicals and minerals have been considered as binder materials in the production of consolidated glass batches. These binders have included paper pulp, cellulose, bentonite and carbonates [12, 13]. Potentially, briquetting can give greater advantages in terms of formation and strength than pelletisation or granulation, since briquettes are formed with the application of external pressure, whereas granules and pellets are gravity-formed with no external pressure applied. Consequently, granules and pellets exhibit greater friability and

lower mechanical strength and cohesion. Consolidated batch and / or cullet can also provide advantages in the furnace such as decreased melting and refining times [5, 9, 13], increased batch thermal conductivity compared with unconsolidated batch materials, shorter batch blankets on the surface of the melt [9] and higher output of glass or "pull rate" [14]. All of these can contribute to lower SEC and fuel consumption and hence lower CO_2 emissions from glass manufacture.

As a reusable raw material, glass fines will have their own characteristic effects on the final glass quality. Bulk glass cullet can have a moderately reducing effect on redox conditions during melting due to organic contamination such as residual foodstuffs, labels and glue, particularly from cullet collected from public bottle banks. This reductive contamination affects the partial pressure of oxygen (pO_2) in and above the glass melt in the furnace, and can in some circumstances lead to problems with final glass colour and refining. Most importantly, glass colour will be affected, as the Fe^{2+}/Fe^{3+} ratio varies with pO_2 [15] and under strongly reducing conditions the well-known Fe^{3+}-S^{2-} amber chromophore can form [16-18]. Under less reducing conditions than those required to form full amber colour, an olive-green colour can form [17, 18]. Such colours may be undesirable if the aim is to manufacture a colourless or green glass. To provide the correct redox balance, oxidizing agents such as sulphates, nitrates and oxides of manganese, cerium, arsenic or antimony can be added to the batch [16-19]. However, a preferable solution is to control the levels of organic cullet contamination, rather than attempt to offset its effects through adding other dopants or oxidizing agents. Compared to bulk cullet, the specific surface area

of glass fines is relatively high and coupled with this, glass fines contain more contamination such as ceramics and organics. Modifying the batch to adapt to these effects, if necessary, is thus a consideration.

In this study, briquetted glass fines were manufactured and tested. A mixture of glass fines with appropriate additions of a binder material and water was formed as briquettes using the application of a mould and pressure. The density, compressive strength and weight loss of the resulting briquettes were investigated as a function of time after briquette formation. For comparative glass melting and property assessments, a representative green container glass batch with 87 wt % cullet was chosen as a benchmark. With compensation of the batch to maintain the same final glass composition with and without briquette additions, glass batches containing different amounts of briquettes were melted, wherein the briquettes partially replaced the regular cullet so as to maintain the same overall recycled glass (briquettes + cullet) percentage. UV-Vis-IR absorption spectroscopy was used to determine the optical absorption spectra, and hence the colour and redox ($Fe^{2+}/\Sigma Fe$) ratio estimation of all glasses.

2. Experimental Procedures

Glass fines, which were originally destined to be sent to landfill, were collected from a German recycled glass supplier. An Olympus BX 51 optical microscope was used to characterize the appearance and constituents (amber, green or colourless glass; ceramics, organics) of received glass fines, prior to briquetting. To enable comparison of as-received glass fines with clean fines, the as-received glass fines were cleaned

using acetone in an ultrasonic bath for 2 minutes. Very thin specimens (about 2mm thick) were prepared for optical microscope. The sieving method was used for glass fines particle sizes distribution measurement, and the particle sizes of the glass fines are given in Figure 1.

Briquettes were manufactured by mixing sodium silicate ($Na_2O{\cdot}2SiO_2$), sodium carbonate (Na_2CO_3), glass fines and water. Briquettes were produced using a proprietary mechanical mixing and forming method which consistently produced briquettes of typical dimensions 20 x 30 x 40 mm. After thorough mixing of the briquette constituents, the mixture was fed into a roller press with moulds on a double roll to compress the mixture into a briquette at applied pressures of approx, 50 MPa. After formation, briquettes then passed along a conveyor belt with heating to partially dry them, and after 2 minutes were deposited from the end of the conveyor into large bags. Briquettes were then collected for analysis.

Measured densities of briquettes, glass and glass fines are shown in Table 2. The bulk density of glass fines was measured 3 times for each sample using a standard density apparatus according to BS EN 459-2:2010. The true density of container glass cullet and glass fines have been measured by the Archimedes method using distilled water as the suspension medium. Densities were calculated using (1):

$$\rho = \left[\frac{\mathbf{W}_A}{\mathbf{W}_A - \mathbf{W}_W}\right]\delta_W \qquad (1)$$

where ρ= density in g cm^{-3}; W_A= weight in air; W_W= weight in water and δ_W = water

density with temperature correction. Bulk density of briquettes was measured by the Archimedes method. To prevent interactions with the measurement medium (water), samples were embedded in paraffin. Briquette densities were calculated using (2):

$$\rho_B = \frac{W_B}{\left[\left(\frac{W_A}{\rho_A}\right) - \left(\frac{W_p}{\rho_p}\right)\right]} \quad (2)$$

where ρ_B= density of briquette in g cm^{-3}; W_B= weight of briquette in air; W_A= weight of paraffin-embedded briquette in air; ρ_A= density of paraffin-embedded briquette, which can be calculated by Archimedes method; W_p= weight of paraffin, which is the weight difference before and after the embedded process and ρ_p= density of paraffin. Weight loss as a function of time after manufacture was measured for 20 briquettes at room temperature (ca. 20 ^oC) using a high-precision 2 decimal place balance. The results are shown in Figure 4. Under identical conditions, the compressive strength of briquettes was measured using an INSTRON 2530-445 (capacity: 50kN) as a function of time since briquette formation, the values provided here being determined as averages value of at least 3 measurements. Results are shown in Figure 5. To characterize the morphology, microstructure and composition of briquettes, samples were coated by ~20 nm carbon film for SEM (FEI Quanta 650) and EDS (Oxford Instruments/line scan mode) characterization.

The representative (benchmark) green container glass batch and modified batches containing briquettes replacing standard cullet that were melted under laboratory conditions, are presented in Table 3. Series One batches were produced, wherein

briquettes partially replaced standard cullet at several levels from 0 to 20 wt %. Sample naming is of the form B-#, where # denotes the amount of briquettes added in weight %. Series Two batches were variants of the Series One B-15 batch, wherein the levels of added colourants were varied in order to provide colouration comparable to the benchmark glass. These samples are denoted B-15a, b, c and d. In addition, samples of as-received glass fines, briquettes and general glass cullet were each re-melted to enable comparative optical absorption measurements. Industrial raw materials and cullet were obtained from a UK container glass manufacturer, and batches were weighed out using a 2 decimal place balance to provide batches weighing 200g. Batches were thoroughly mixed and were then placed in recrystallized Al_2O_3 crucibles. Crucibles were heated in an electric furnace at a rate of 4^oC / minute to 1450^oC and then held at this temperature for 4h. Crucibles were then removed from the furnace and the molten glass poured into a stainless steel mould and allowed to cool until sufficiently rigid to remove the mould. The glass was then annealed at 520^oC for 1h, then cooled slowly to room temperature. Resulting glass compositions were determined using X-ray fluorescence spectroscopy (wavelength dispersive Philips PW2440 sequential X-ray fluorescence spectrometer) and results are presented in Table 3. Uncertainties associated with the XRF analyses are estimated at ±2% of measured concentrations.

Glass samples were prepared for optical spectroscopy measurement by grinding using successively finer SiC grinding pads from 60 to 1200 grit size, then polished using a suspension of CeO_2 powder in water to provide a highly polished (< 1µm)

surface finish. Optical absorption spectra were measured using a Varian 50Scan UV-Visible-near-IR spectrophotometer over the wavelength range 300-1000 nm. The repeatability of measured absorbance data was confirmed by measuring each sample 3 times.

3. Results

The glass batch compositions used in this research are given in Table 1 (a) and (b). Owing to the presence of binder materials in briquettes, and in order to keep the final target glass composition unchanged, briquette-containing glass batches were modified slightly. For Series One batches, sample B-15 is close to the upper limit for achieving an unchanged nominal final glass composition, whilst sample B-20X presents a slightly elevated Na_2O content in the final glass, despite removing all Na_2CO_3 from the raw materials, due to the binders present in the briquettes used. Series Two batches B-15a, b, c, d, with modification of colourant and oxidant constituents are shown in Table 1 (b). Manganese ore and chromite contents were varied. XRF analyses of final glasses are shown in Table 2. This confirms, within experimental uncertainties, that the chemical composition of the benchmark glass was largely maintained for B-9 and B-15 glasses, however, small increases in SiO_2 content are likely to have resulted from corresponding small differences in SiO_2 and CaO content of glass fines compared with cullet. Further batch modification would be required to fine-tune this, for example by slightly increasing the limestone contents of briquette-containing batches. Such modifications are regularly carried out in the glass

industry.

The particle size distribution (PSD) of the glass fines is given in Figure 1. There were no particles larger than 2 mm diameter; 37.8 wt % were between 0.5 and 2 mm; 46.8 wt % between 0.25 and 0.5 mm; 11 wt % between 0.125 and 0.25 mm; 3.2 wt % between 0.125 and 0.062 mm, and the balance (1.6 wt%) smaller than 0.062mm. Figure 2 shows optical micrographs of glass fines before and after cleaning in acetone. Under optical microscopy, fines are shown to be a mixture of amber, flint and green glass particles. For the as-received samples, considerable levels of contaminants are observed. A simple loss-on-ignition (LOI) analysis of raw glass fines was carried out by heating 10 g of glass fines at 100 ^{o}C and 700 ^{o}C each for 3h, and showed a moisture loss of 0.13 ± 0.04 wt % at 100^{o}C and a total weight loss of 0.75 ± 0.07 wt% at 700^{o}C. Considering their relatively low density, these organic contaminants impact on redox and are discussed in Section 4. The optical and secondary electron SEM micrographs of briquette cross-sections are presented in Fig. 3a and Fig. 3b. Briquettes exhibit a dense and compact microstructure. The EDS line scan shows a continuous phase - glass particle interface in briquettes (Fig. 3c and 3d).

Note from Richard. Should we mention something here about the fines needing to be at 1 mm or less because of CSP inclusions. During residence time in glass melting these can dilute into the bath causing no reduction in final quality

The bulk and true densities of standard cullet, glass fines and briquettes are shown in Table 3. The true density of glass fines (2.513 g/cm^3) is close to that of standard cullet (2.544 g/cm^3), as would be expected. For the porous and powder form, glass fines

contain a lot of air, the bulk density of glass fines is, however, very low as would be expected. Yet bulk density increased from 1.311 to 2.105 g/cm^3 after briquetting. This is consistent with the optical microscopy results in Fig. 2, which confirm that the contact area of glass fines in briquettes is greatly increased, and thus the voids / porosity are substantially decreased. This suggests that thermal conductivity of briquettes should be substantially greater than unconsolidated glass fines. The thermal conductivity of glass batch was measured over the range 100^{o}C to 1250^{o}C by Kröger and Eligehausen [20]. More recently, further data on thermal conductivity of glass batches were reported by Verheijen *et al.* [21], Schill [22] and Hrma *et al.* [23]. Their studies focused on the precise measurement of effective thermal conductivities in different glass batches. A gradually linear increase of thermal conductivity was observed from ~100^{o}C to ~650^{o}C, before a sudden rapid increase above 700~750^{o}C which may be due to liquid phase formation [21, 23]. The thermal conductivity of loose (unconsolidated) glass batch at room temperature is 0.273 W/m·°C. It was increased to 0.430 W/m·°C as the bulk density increased from 1.291 g/cm^3 to 2.124 g/cm^3 by compression (consolidation) of the batch [24]. Meanwhile, the thermal diffusivity of cullet is always higher than that of virgin glass batch during heating [25]. Thus, as a consolidation method, briquetting of glass fines can provide a net increase in thermal conductivity compared with loose glass fines.

In Figure 4, weight loss curves of 20 briquettes at room temperature are presented. They show that, although the briquettes have the same nominal composition and are produced under essentially the same conditions, weight loss rates vary somewhat for

241 different briquettes.

242 Figure 5 shows the measured compressive strength of briquettes as a function of
243 time from formation. The initial strength of briquettes is relatively low and not more
244 than 5 MPa in the first 5 days, rising to ~60 MPa after 30 days.

245 UV-Vis-IR absorption spectra of benchmark glass, melted glass fines, melted
246 briquettes and melted standard cullet within the wavelength range of 300-1000 nm are
247 presented in Figure 6a. For every curve, the UV absorption edge is near 370 nm, and
248 spectra contain one narrow absorption band at 380 nm and two wider absorption
249 bands centered at ca. 450 nm and 660 – 700 nm. Compared to the benchmark glass,
250 the absorbance of melted glass fines, briquettes and standard cullet in the visible
251 region (ca. 400 – 650 nm) is lower. A broad optical absorption band centered at a
252 wavelength of ~1100 nm was also observed in melted glass fines, melted briquette
253 and melted general cullet samples. As shown in Figure 6b, the absorption spectrum of
254 samples B-0, B-9, B-15 and B-20X are almost the same. In Figure 6c, the absorption
255 spectra of samples B-15a, b, c and d, produced with varying amount of manganese ore
256 and chrome premix additions, are presented. The strength of the absorption bands
257 centered at 450 nm and 660-700 nm in samples B-15a and B-15b are lower than that
258 of sample B-15, and the broad absorption band centered at ~1100 nm in sample B-15a
259 is present. Meanwhile, the absorption spectrum of sample B-15c is similar to sample
260 B-15 at < 700 nm, however, at wavelengths above 700 nm, the absorption strength of
261 sample B-15c increases. For the sample B-15d spectrum, the absorbance below ~700
262 nm is relatively low and above 700 nm it is relatively high compared to sample B-15.

4. Discussion

4.1. Briquettes

As described in Sections 1 and 2, a small particle size is the biggest obstacle for the recycling of glass cullet fines into glass furnaces. A screen classification method was used to investigate the particle size distribution of the glass fines studied here. From Figure 1, the particle size distribution of glass fines is not a normal distribution: this can be explained because larger particles are routinely separated and extracted by cullet suppliers. No particle is larger than 2mm. These glass fines will carry entrained air into the glass furnace and hence into the melt, not only increasing furnace dusting [5] and reducing the thermal conductivity of the batch blanket [5], but also causing melt foaming and making satisfactory melt refining more difficult [5-7].

As a glass batch raw material, the components of glass fines need to be understood. For standard bulk glass cullet, the proportions of amber, green and colourless cullet and organic contamination can now be closely controlled [9]. The chemical composition of different colours of bulk cullet is similar, except for the colorants and, in certain cases, SO_3 contents. To investigate cullet composition, we re-melted standard bulk cullet and compared it with re-melted glass fines using XRF. As shown in Table 3, XRF analyses of remelted cullet and remelted glass fines are similar, especially for colouring agents Cr_2O_3, MnO and Fe_2O_3. This supports the view that re-introduction of glass fines into glass batches can be achieved without the need for substantial modification of batch composition.

In Figure 2, the morphology of glass fines, studied by optical microscopy, is demonstrated. For the raw glass fines in Fig.2a, ultra-fine particles and contaminants also accompany the glass fines. The ultra-fine particles cause dispersion and make the luminous environment, observed under white light, complex. However, it is still possible to distinguish individual amber, green and colourless glass fine particles. After washing in acetone, the cleaned glass fines are presented in Fig.2b. The ultrafine particles and contaminants have been removed and very clean glass particles can be observed, again highlighting the presence of colourless, green and amber glass particles. This is expected at some level for all bottle bank cullet, which may be sorted or unsorted by colour.

From Table 3, the bulk density of briquettes is obviously higher than that of glass fines and close to the real density of bulk glass. The compressive process of briquette manufacture removes voids and entrained air between glass particles effectively and also introduces the binder constituents into some of the existing void space. The briquette cross-section is characterized by optical microscopy and SEM in Fig. 3a and 3b. Glass fine particles are encased in a continuous, dense structure, with binder materials effectively holding the fine glass particles together whilst removing porosity. To demonstrate the interface between the binder phase and glass particles, an SEM image is shown in Fig. 3c. An EDS line scan was performed and the quantitative result is shown in Fig. 3d. The Na and C contents in the binder phase are higher than the surrounding glass fines; and the Si content is higher in the glass fines than in the binder phase. This is fully consistent with the binder phase ingredients ($Na_2O.2SiO_2$

307 and Na_2CO_3). There is no evidence of extensive chemical interaction between binder
308 and glass fines phases, however, the “pore-filling” action of the binder phase can be
309 clearly seen.

310 It has long been known that sodium silicate can be used in sand casting processes
311 as a highly effective inorganic binder to provide high strength performance [26, 27].
312 Here, briquettes required a binder that provide this function but also require strength
313 after forming to enable problem-free transport into the furnace without fragmentation
314 or excessive friability. Thus, sodium silicate was introduced as binder component here.
315 Theoretically, the chemical reaction of sodium silicate-bonded, CO_2 hardened sand
316 system, or the so called “silicate-CO_2 process” [27] can be expressed as (3):

317

318 $$Na_2SiO_3 + CO_2 + H_2O \rightarrow H_2SiO_3 + Na_2CO_3 \quad (3)$$

319

320 The formation of amorphous silica gel from sodium silicate as in (3) requires
321 water and CO_2 from air, but also time for solidification. As a batch component here,
322 water was introduced into the briquetting process to improve the rheology of glass
323 fines and binder mixtures during the briquetting process. However, too much residual
324 water may delay the solidification time, reduce the strength, or even make the
325 briquette thixotropic. Therefore it had to be carefully controlled to ensure
326 problem-free briquette manufacture.

327 Figure 4 shows the weight loss of 20 briquettes as a function of time after
328 formation, to understand drying and hydration reactions with time. After storage at

329 room temperature (ca. 20 ^{o}C) for approximately 150 hours, weight loss reaches a
330 steady state and further weight loss becomes very slow. In Fig.7 a), the instant weight
331 loss rates (R_I) of different briquettes are presented and calculated with weight
332 difference between adjacent measurements divided by time. The initial rates are
333 relatively fast in the first 75 hours, then the loss rates fluctuate around +/-0.005 wt% /
334 h. Interestingly, some variability is observed in weight loss curves for different
335 briquettes. In Fig.7 b), the average weight loss rates (R_a) of 20 briquettes after 187
336 hours are demonstrated as the function of briquettes initial weight, and calculated with
337 weight difference between the current and initial measurement divided by the time.
338 Weight loss rates decreased with increasing of initial weight. This shows that water
339 removal from a heavy briquette is slower than for a lighter briquette. Briquette sizes
340 did vary, owing to the method of formation, with some being thicker and others
341 thinner. This result strongly suggests that weight loss differences are due to
342 differences in surface area to volume (SA/V) ratio, i.e. lighter briquettes have a larger
343 SA/V ratio and therefore water removal (drying) is more rapid compared to heavier
344 briquettes. In Fig.7 c), the relationships between initial weight of briquettes and
345 average weight loss rate at different time are presented. The average weight loss rates
346 are similar to one another and the influence of initial weight on the weight loss rate is
347 gradually reduced. Clearly water evaporation plays a primary role on the weight loss
348 during this period. However, the reaction of sodium silicate in the binder with CO_2
349 from air, carbonation [27], also needs to be considered because this process will
350 slightly increase the weight of briquette.

Compressive strength of briquettes increases linearly as a function of time after formation, as shown in Figure 5. The carbonation of sodium silicate needs time to form silica gel similarly to hydration of concrete from a dynamic viewpoint [28].

4.2. Composition, colour and redox of glass

Since the composition of recycled glass cullet is similar to the composition of the glass fines (Table 3b), briquettes can be added into the batch whilst changes in the accompanying glass batch can compensate for the extra Na_2O and SiO_2 arising from the binders. With precise design, the chemical composition of Base line, B-9 and B-15 glasses are closely similar, with those differences that do arise being attributable to cullet and glass fines impurities and compositional differences, and to uncertainties associated with the XRF analyses. For sample B-20X, it was not possible to fully balance the additional Na_2O and Na_2CO_3 from the briquette binder by removing batch Na_2CO_3, and consequently the Na_2O content of this glass is higher than the benchmark. However, the other ingredients in B-20X are as same as in the Base Line sample.

As described in Section 1, batch redox plays an important role in glass manufacture, particularly in the preparation of homogeneous glass free from bubbles and in making colored glasses containing transition metal ions [29]. For some transition metal ions UV-Vis absorption spectra can not only characterize the colour properties of glass in the visible light region, but also the redox of different glasses can be deduced and compared from the relative intensity of optical absorption spectra.

373 It is well known that glass redox status can be estimated through the Fe^{2+}/Fe^{3+} or
374 $Fe^{2+}/\Sigma Fe$ ratio [30-32]. As a colourant ion, Fe^{2+} gives a stronger blue colour in silicate
375 glass whilst Fe^{3+} gives a weaker yellow-green colour [33]. The $Fe^{2+}/\Sigma Fe$ ratio gives an
376 indication of the oxidation state of the glass [15]. According to ligand field theory, the
377 absorbance peaks due to *d-d* transitions of Fe^{2+} and Fe^{3+} were summarized previously
378 [30, 34]. In Fig.6 a), the absorption spectra of Base Line, remelted briquette, remelted
379 cullet and remelted glass fines samples are presented. The optical absorption band
380 centred at~380 nm is attributable to the $^6A_1(S)\rightarrow{}^4E(D)$ transition of tetrahedrally
381 coordinated Fe^{3+} cations. The intensity of this band is positively associated with the
382 concentration of Fe^{3+}. For remelted briquette, cullet and glass fine samples, a broad
383 optical absorption band centered at a wavelength of slightly higher than 1000 nm is
384 attributable to the $^5A_2(S)\rightarrow{}^5E(D)$ transition of octahedrally coordinated Fe^{2+} cations.
385 The increase in intensity of this band for the remelted briquette, cullet and glass fines
386 samples compared with the Base Line glass, coupled with the opposing trend of
387 decreasing intensity of the Fe^{3+} band at 380nm, confirms that the $Fe^{2+}/\Sigma Fe$ ratio is
388 higher in the remelted briquette, cullet and cullet fines samples than the Base Line
389 glass. In the UV edge part of spectrum, there are strong UV peaks from Fe^{2+} (centered
390 ~214 nm) and Fe^{3+} (centered ~254 nm), which are caused by the charge transfer of 3d
391 to 4s[30]. The UV edge intensity increases and moves towards longer wavelengths
392 with decreasing $Fe^{2+}/\sum Fe$ ratio, i.e. with increasing oxidation of the melt. Organic
393 contamination in recycled cullet or glass fines shifts the redox equilibrium $Fe^{2+}\leftrightarrow$
394 Fe^{3+} to the left in the glass melting furnace, increasing the $Fe^{2+}/\sum$ Fe ratio.

For chromium, Cr^{3+} exhibits a distinctive absorption spectrum with a split, broad band centred at 660-700nm attributable to the $A_{2g}(F) \rightarrow {}^4E_{2g}(F)$ transition; and another band with similar intensity occurring at ~450 nm, attributable to the $A_{2g}(F) \rightarrow {}^4E_{1g}(F)$ transition [35]. If these recycled cullet/fines or briquettes are reused in glass batch, the compensation of chromium must be set up for the glass colour correction in visible wavelength range.

In industrial production, colour and redox state of commercial glasses are usually controlled by the use of oxidizing/ reducing batch constituents, furnace atmosphere and colorants. The redox and colour of glass batches with different amount of briquette studied here was controlled by modification of the manganese ore and chrome premix batch components. In Fig.6b, the absorption spectra of sample Base-line, B-9, B-15 and B-20X are presented. After careful modification, the glasses produced from batches with increasing briquette contents (B-9, B-15 and B-20X) show the same spectral features as the Base line sample and, crucially, the absorption profiles of all samples closely match that of the base line glass, in terms of both spectral profile and quantitatively in terms of absorbance. This is consistent with the colourant (Fe, Cr, Mn) contents of these glasses, which also show no variation within uncertainties of analysis. Consequently, it can be surmised that samples B-9, B-15 and B-20X all have closely similar $Fe^{2+}/\Sigma Fe$ redox ratios to the base line glass, and all show low $Fe^{2+}/\Sigma Fe$, indicating oxidized glasses. The effects of the manganese ore and chrome premix batch additions were also studied for Series Two glasses, B-15a to B-15d. The main colourant / redox-active components of these raw materials are

417 MnO_2 from manganese ore, and both Cr_2O_3 and Fe_2O_3 from chrome premix. The
418 compositions of B-15a to B-15d are listed in Table 3 and their absorption spectra are
419 shown in Fig.6c. With no manganese ore of chrome premix added, sample B-15a
420 shows the same spectral features as the remelted cullet or remelted glass fines samples
421 in Fig. 6a, which shows that B-15a has a higher $Fe^{2+}/\Sigma Fe$ ratio (i.e. more reduced).
422 With insufficient compensation of colorant agents (Manganese ore and Chrome
423 premix), the spectrum characteristic of B-15b between B-15 and B-15a.

424 Manganese in silicate glass normally distributes into Mn^{2+} and Mn^{3+} and
425 generates the absorption band centred at ~500 nm (purple colour) due to Mn^{3+} [36],
426 which undergoes mutual redox interactions with Fe^{2+}, thereby reducing to the
427 colourless Mn^{2+} whilst oxidising iron to the weakly yellow/green-coloured Fe^{3+}.
428 Small amounts of manganese were introduced because of this oxidising ability. For
429 sample B-15c, the visible absorption spectrum is almost the same as sample B-15.
430 However, due to the absence of Mn ore in the batch for this sample, the broad optical
431 absorption band centered at ~1100 nm (Fe^{2+}) is stronger, hence the glass is more
432 reduced and the IR absorption greater. For sample B-15d, the low Cr not only causes
433 the low absorption at 660 - 700 nm and ~450 nm, but also higher absorption at ~1100
434 nm (Fe^{2+}).

435

436 **5. Conclusions**

437 Briquettes consisting of 82 wt % recycled glass fines were made with additions of
438 sodium silicate, sodium carbonate and water. Briquette bulk density (2.105 g/cm^3) is

higher than that of the glass fines (1.311 g/cm^3), as expected. There is faster mass loss (~-0.06 wt%/h) due to evaporation in the 24 hours following briquette production, and further mass loss due to evaporation is considerably slower (~-0.005 wt%/h) thereafter. There is also a negative correlation between the initial briquette mass and moisture evaporation rate. The compressive strength of briquettes increases linearly with time, increasing from 2 MPa to 60-65 MPa after 33 days at room temperature (ca. 20^{o}C) and ambient humidity. With compensation of the glass batch materials to maintain a consistent nominal final glass composition, up to 15 wt % briquettes can be added to the batch. These batches rapidly melted to form glasses with comparable properties to briquette-free benchmark glasses. UV-Vis-near IR absorption spectra confirmed that the colour and redox state of resulting glasses can be maintained for different briquette additions. It is thus demonstrated that commercial SLS glasses produced using up to 15 wt% briquetted glass cullet fines exhibit comparable compositions and properties to SLS glasses produced using briquette-free batches, supporting the potential use of this technology for enhanced energy and resource efficiency, and lower CO_2 emissions, from commercial glass manufacture.

Acknowledgements

The authors acknowledge financial support from EPSRC under grant EP/P510725/1 and Innovate UK under grant 63406-429275. The authors appreciate useful discussions with Vincenzo Starinieri, Francis Clegg, Anthony Bell, Paul Allender, Tim O'Hara and James Burke.

Reference

1. Ruth, M., Dell'Anno, P. An industrial ecology of the US glass industry. *Resources Policy*, 1997. **23**(3): p. 109-124.
2. Hartley, A. A study of the balance between furnace operating parameters and recycled glass in glass melting furnaces. 2004, *Glass Technology Services Ltd*.
3. Deng, W., et al. Research of Sintering Reactions Process and heat Calculation in Glass batch. *J. Wuhan Univ. Technol.*, 2010. **22**: p. 111-113.
4. Kovacec M., Pilipovic A., Stefanic N. Impact of glass cullet on the consumption of energy and environment in the production of glass packaging material. *Recent Researches in Chemistry, Biology, Environment and Culture. Monteux, Switzerland,*. 2011.
5. Cable, M. A Century of Developments in Glassmelting Research. *J. Am. Chem. Soc.*, 1998. **81**(5): p. 1083-1094.
6. Schaeffer, H.A. Recycling of cullet and filter dust in the German glass industry. *Glass Sci. Technol.*, 1996. **69**: p. 101-106.
7. Ross, C.P. Glass Science Tutorial: Lecture #4, Commercial Glass Melting and Associated Air Emission Issues, *U.S. DOE Office*, Editor. Jan. 1995.
8. Bertuzzi, P., Ercole, P., Ferrero C., Ramon, L. Glassy sand from cullet rejected during primary processing: quality, energy and environmental analysis. in *glass machinery plants & accessories* 2009, Smartenergy S.r.l. p. 6.
9. Hamdan, K.A., Hessenkemper, H., Wiltzsch, S. New Developments of Batch Briquetting, in *74th Conference on Glass Problems*. 2014, *John Wiley & Sons, Inc*. p. 33-42.
10. Misra, V.N., Reddy, P., Mohapatra, B. Mineral Characterisation and Processing. 2004: *Allied Publishers*.
11. Garkavi, M.S., Kulaeva, N.S. Technological parameters of briquetting batch for foam glass production. *Glass and Ceramics*, 2005. **62**(11): p. 379-380.
12. Bai, X., Jia, D., Cheng, B.W., Zhao, H.L., Liang, X.P. The influence of the Binders on Compaction of Glass batch. *B. Chin. Ceram. Soc*., 2009. **28**(3): p. 585-588.
13. Krasheninnikova, N.S., Frolova, I.V., Vereshchagin, V.I. Application of Granulated Raw Concentrate in Glass Technology. *Glass and Ceramics*, 2004. **61**(5): p. 164-167.
14. Beerkens, R., Energy saving options for glass furnaces & recovery of heat from their flue gases and experiences with batch & cullet pre-heaters applied in the glass industry. *in 69th Conference on Glass Problems: Ceramic Engineering and Science Proceedings*, C.H. Drummond, Editor. 2009, John Wiley & Sons, Inc.: Hoboken, NJ, USA. .
15. Simpson, W., Myers, D. The Redox Number Concept and Its Use by the Glass Technologist. *Glass Technol.*, 1978. **19**: p. 82-85.
16. Goldman, D.S., Oxidation Equilibrium of Iron in Borosilicate Glass. *J. Am. Chem. Soc.*, 1983. **66**(3): p. 205-209.
17. Shi, X.Y., Brungs, M.P., Young, D.J. The iron redox couple and its interaction with sulphur in glass. *Phys. Chem. Glasses*, 1995. **36**(6): p. 275-278.
18. Beerkens, R. Amber chromophore formation in sulphur- and iron-containing soda-lime-silica glasses. *Glass Sci. Technol.* 2003. **76**(4): p. 166-175.
19. Shelby, J.E., Introduction to Glass Science and Technology. 2005: *Royal Society of Chemistry.*
20. Kröger, C., Eligehausen. H. *Über das Wärmeleitvermögen des einschmelzenden*

Glasgemenges. Glastechn. Ber., 1959. **9**(32): p. 362-373.
21. Verheijen, O., Beerkens, R., Op den Camp. O. Thermal heat conductivity of glass forming batches. *in Glass Odyssey: Proc. Sixth ESG Conf.* 2002.
22. Schill, P., Lutze, W. Modeling the behavior of noble metals during HLW vitrification in the DM1200 melter, *VSL-05R5740-1*, Vitreous State Laboratory, Washington DC, 2005.
23. Pokorny, R., et al. Determination of temperature-dependent heat conductivity and thermal diffusivity of waste glass melter feed. *J. Am. Chem. Soc.*, 2013. **96**(6): p. 1891-1898.
24. Wang, J., et al. Melting properties of loose and granulated glass batch. *J. Wuhan Univ. Technol.-Mater. Sci. Ed.*, 2014. **29**(6): p. 1161-1164.
25. Faber, A.J., Beerkens, R., Waal, H.d. Thermal behaviour of glass batch on batch heating. *Glastech. Ber.*, 1992. **65**(7): p. 177-185.
26. Parappagoudar, M., Pratihar, D., Datta, G. Neural network-based approaches for forward and reverse mappings of sodium silicate-bonded, carbon dioxide gas hardened moulding sand system. *Materials and Manufacturing Processes*, 2008. **24**(1): p. 59-67.
27. Owusu, Y.A. Physical-chemistry study of sodium silicate as a foundry sand binder. *Adv. Colloid Interface Sci.*, 1982. **18**(1): p. 57-91.
28. Chang, C.F., Chen J.W. The experimental investigation of concrete carbonation depth. *Cem. Concr. Res.*, 2006. **36**(9): p. 1760-1767.
29. Paul, A., Oxidation — Reduction Equilibrium in Glass Forming Melts, in Amorphous Magnetism II, *R.A. Levy and R. Hasegawa, Editors.* 1977, Springer US: Boston, MA. p. 597-611.
30. Bingham, P.A. The environment of iron in silicate glasses, in Materials Science and Engineering. 2001, University of Sheffield.
31. Wright, A.C., Clarke, S.J., Howard, C.K., Bingham, P.A., et al. The environment of Fe2+/Fe3+ cations in a soda-lime-silica glass. *Physics and Chemistry of Glasses : European Journal of Glass Science and Technology Part B*, 2014. **55**(6): p. 243-252.
32. Bingham, P.A., et al. Redox and clustering of iron in silicate glasses. *J. Non-Cryst. Solids*, 1999. **253**(1–3): p. 203-209.
33. Volotinen, T.T. Mathematical description of absorbance spectra fo Fe and Cu doped soda-line-silica glasses, in *The Department of Engineering materials*. 2007, The University of Sheffield.
34. Bingham, P.A., et al., Novel structural behaviour of iron in alkali–alkaline-earth–silica glasses. *Comptes Rendus Chimie*, 2002. **5**(11): p. 787-796.
35. Bingham, P.A, Connelly, A.J., Hand, R.J., Hyatt, N.C., Northrup, P.A., Alonso Mori, R., Glatzel, P., Kavcic, M., Zitnik, M., Bucar, K., Edge, R. A multi-spectroscopic investigation of sulphur speciation in silicate glasses and slags. *Glass Technol.*, 2010. **51**(2): p. 63-80.
36. Thiemsorn, W., et al., Redox ratio and optical absorption of polyvalent ions in industrial glasses. *Bull. Mater. Sci.*, 2007. **30**(5): p. 487-495.

Table 1. Batch compositions of sample glasses

a)

	Baseline Wt %	B-9 Wt %	B-15 Wt %	B-20X Wt %
Other ingredients (sand, limestone, dolomite etc.)	12.53	11.37	10.63	10.35
Cullet	87.47	79.54	74.47	69.75
Briquette	0	9.09	14.9	19.9
SUM	100	100	100	100

b)

	B-15a Wt %	B-15b Wt %	B-15c Wt %	B-15d Wt %
	No colorant	No colorant for briquette	No Mn	No Cr
Other ingredients	9.51	9.51	9.51	9.51
Chrome premix	0	0.81	0.94	/
Manganese ore	0	0.15	/	0.18
Cullet	74.47	74.47	74.47	74.47
Briquette	14.9	14.9	14.9	14.9
SUM	98.88	99.84	99.82	99.06

Table 2. Bulk and true densities of container glass, glass fine and briquette.

	Container glass	Glass fines	Briquette
Bulk density (g/cm^3)	2.544	1.311	2.105
True density (g/cm^3)	2.544	2.513	n/m *

* The true density of briquette cannot be measured as the binder is water soluble.

Table 3. a) Series One XRF analysed glass compositions in wt % (the nominal composition of B-9, 15, 20x should be the same as Base line)

	Baseline	B-9	B-15	B-20X	Cullet	Glass fines	Briquettes
Na_2O	13.24	13.63	13.53	14.71	13.64	13.18	16.54
MgO	1.97	1.85	1.98	1.91	1.31	1.84	1.76
Al_2O_3	2.78	2.89	2.85	2.71	2.99	2.57	1.73
SiO_2	69.53	69.58	70.09	69.01	71.09	71.56	69.18
K_2O	1.10	0.88	0.85	0.81	0.82	0.89	0.72
CaO	9.92	9.63	9.32	9.34	9.31	9.13	9.48
Cr_2O_3	0.38	0.39	0.38	0.39	0.10	0.10	0.12
MnO	0.18	0.19	0.18	0.19	0.07	0.05	\
Fe_2O_3	0.57	0.59	0.53	0.57	0.40	0.34	0.34
SO_3	0.09	0.17	0.08	0.12	0.06	0.04	0.04
P_2O_5	\	\	\	\	0.03	0.03	\
TiO_2	0.09	\	\	\	\	0.07	\
SrO	0.08	0.10	0.10	0.10	0.02	0.03	\
BaO	0.07	0.07	0.07	0.08	0.10	0.13	0.07
Cl	\	0.03	0.04	0.06	0.03	\	\
PbO	\	\	\	\	\	0.04	0.02
SUM	100	100	100	100	100	100	100

Table 3. b) Series Two XRF analysed glass compositions in wt %

	B-15a	B-15b	B-15c	B-15d
Na_2O	13.54	13.46	13.51	13.45
MgO	1.87	1.87	1.86	1.84
Al_2O_3	3.19	3.18	3.13	3.14
SiO_2	70.12	70.05	70.00	70.20
K_2O	0.87	0.86	0.83	0.87
CaO	9.39	9.36	9.32	9.27
Cr_2O_3	0.11	0.23	0.37	0.15
MnO	0.06	0.14	0.07	0.19
Fe_2O_3	0.48	0.49	0.50	0.48
SO_3	0.09	0.09	0.10	0.09
P_2O_5	\	\	\	\
TiO_2	0.07	0.07	0.07	0.07
SrO	0.09	0.08	0.08	0.10
BaO	0.07	0.08	0.09	0.09
Cl	0.03	0.02	0.04	0.03
PbO	0.02	0.02	0.03	0.03
TOTAL	100	100	100	100

Figure 1. Analyzed particle size distribution of glass fines

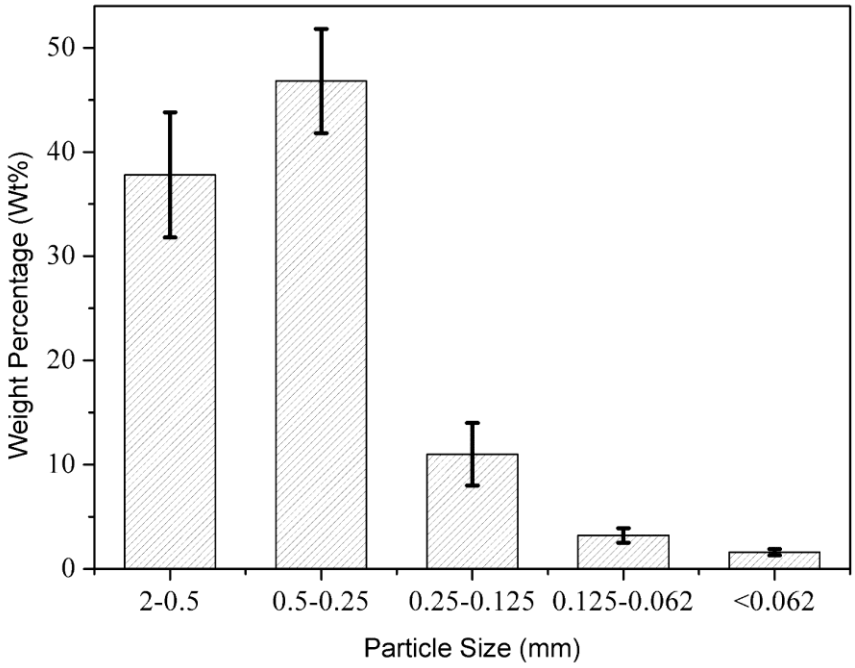

Figure 2. a) Optical micrographs of recycled glass fines; b) Optical micrographs of recycled glass fines washed by acetone in ultrasonic bath for 2mins and then dried.

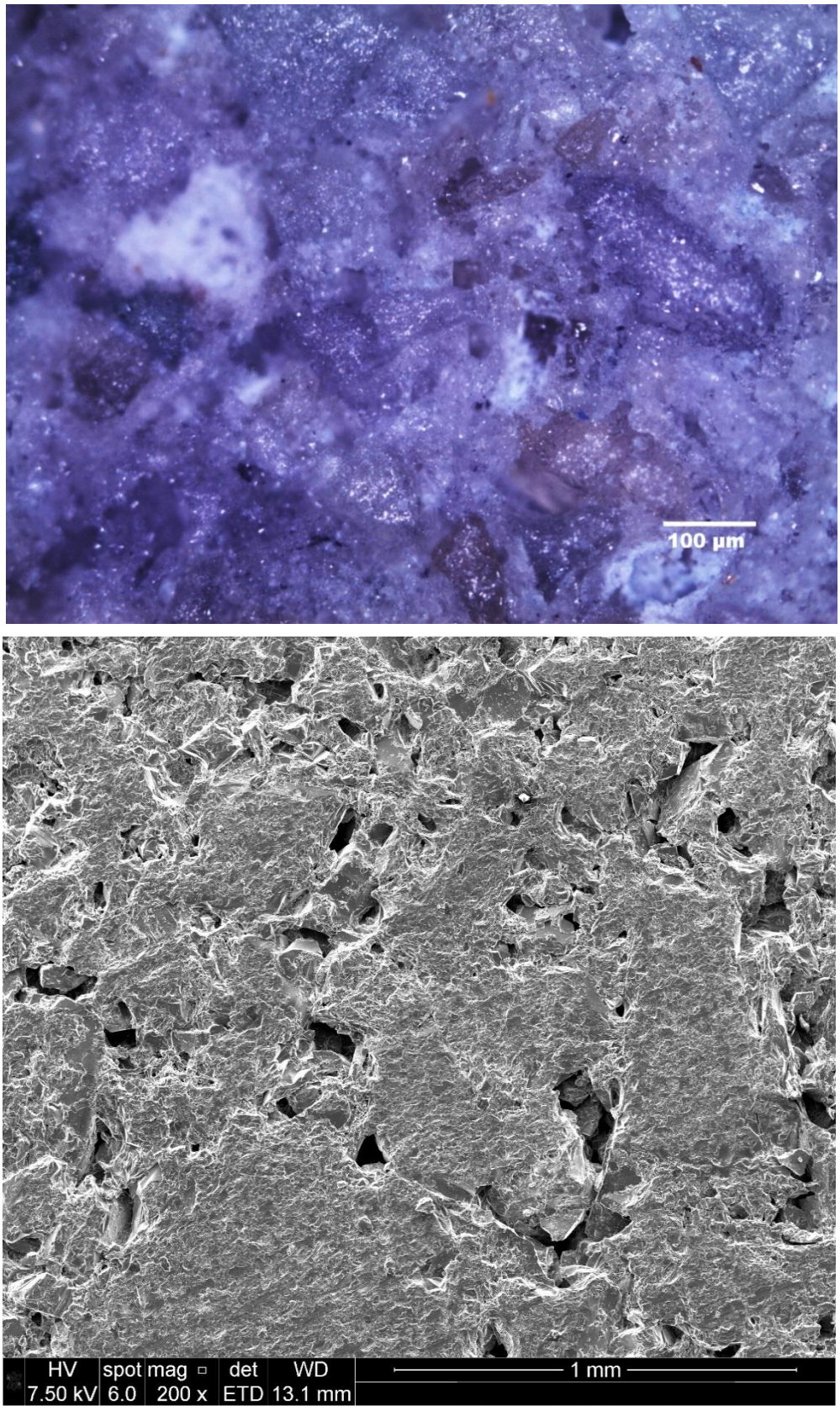

Figure 3.a) Optical and b) Secondary electron SEM images of briquette surface x 200.

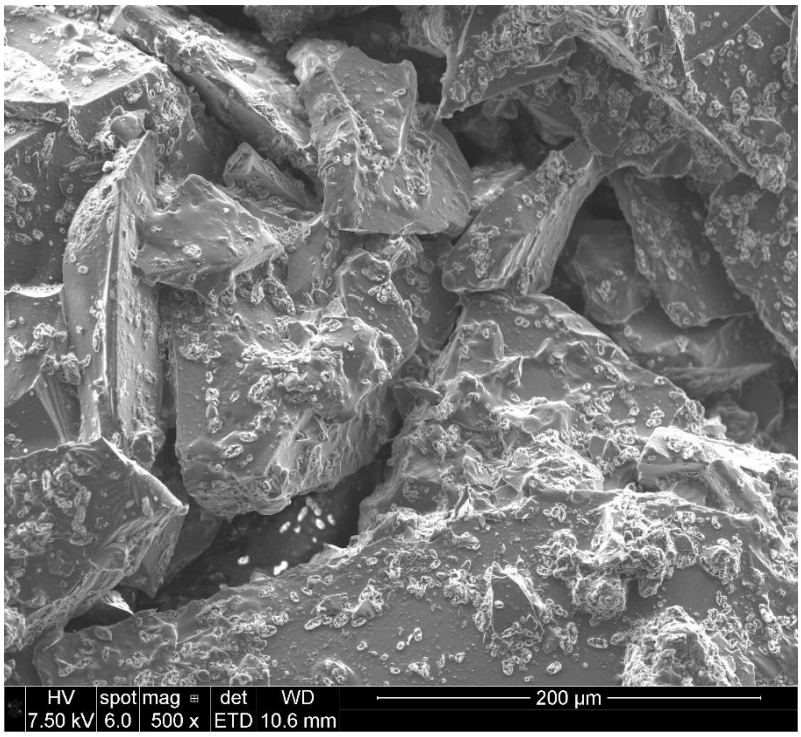

Figure 3.c) Secondary electron SEM image of briquette cross-section x 500.

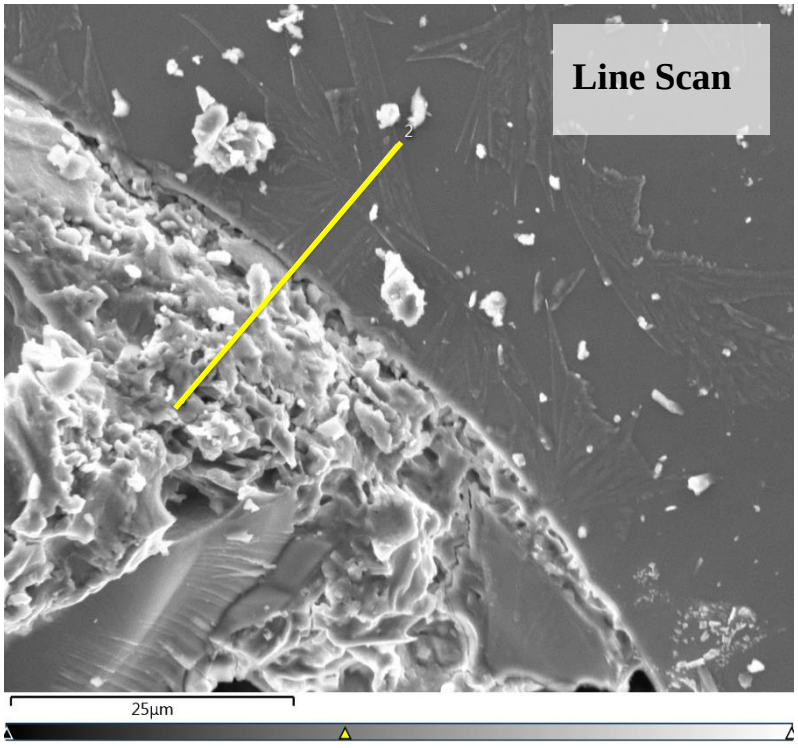

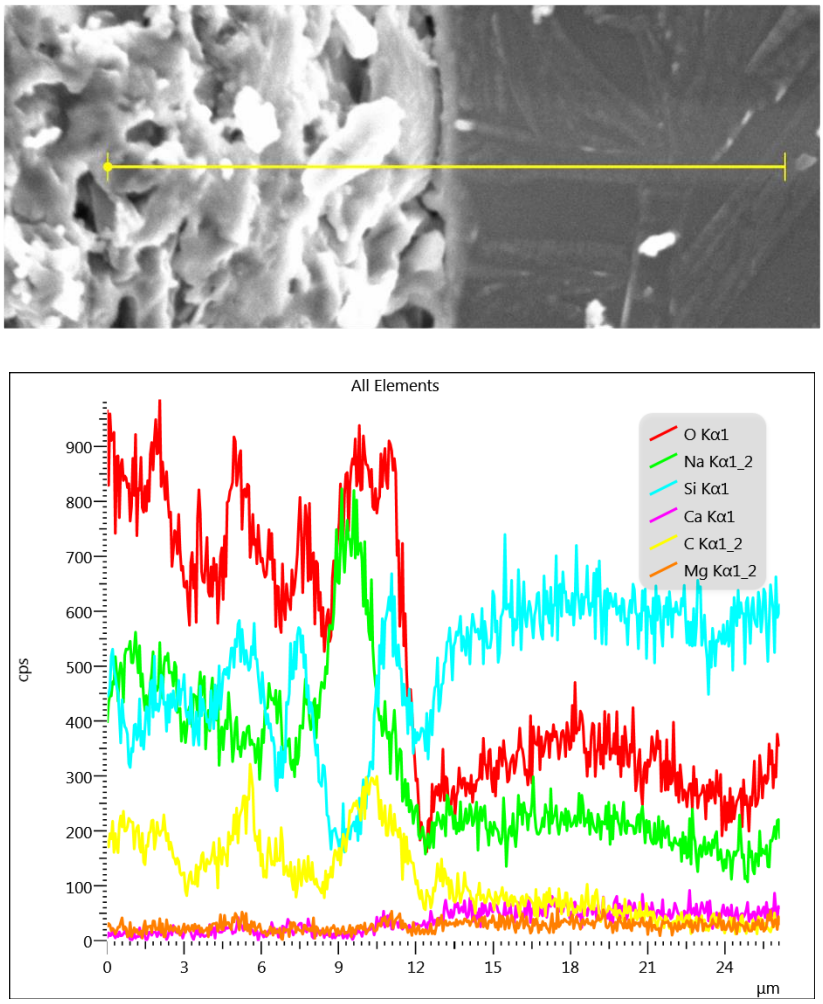

Figure 3.d) EDS line scan result of continuous phase / glass particle interface in briquette.

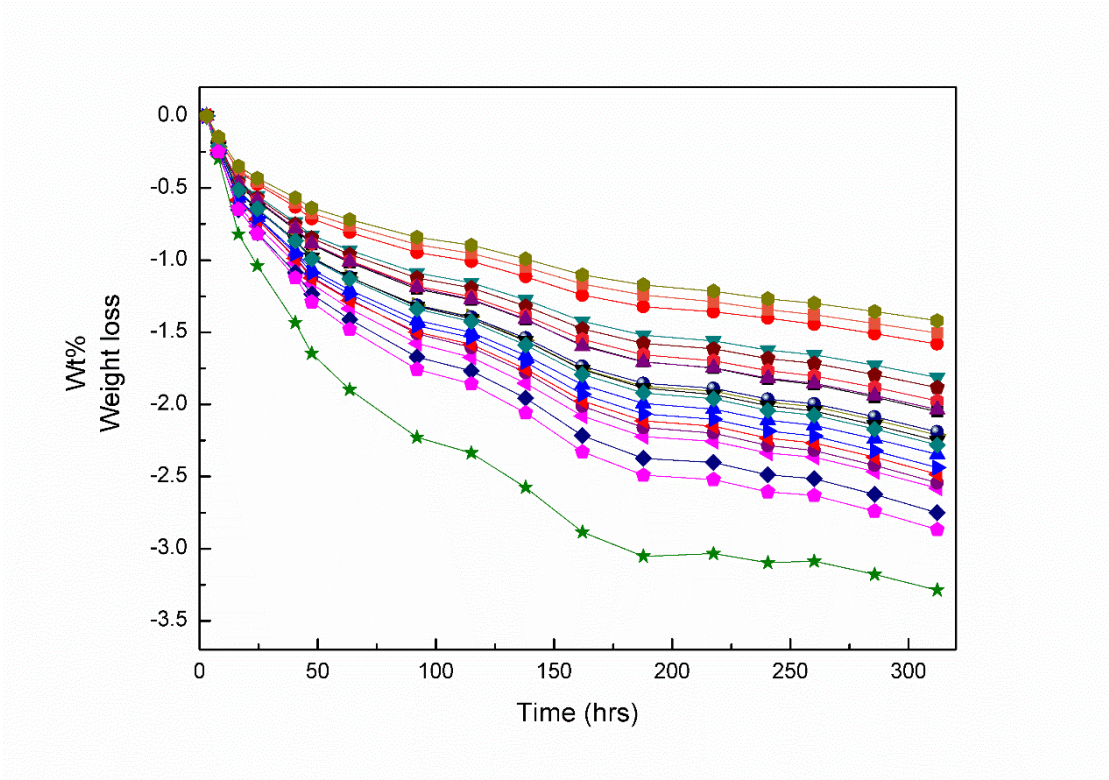

Figure 4. Briquette weight loss as *fn.* (time after forming) for 20 briquettes at room temperature.

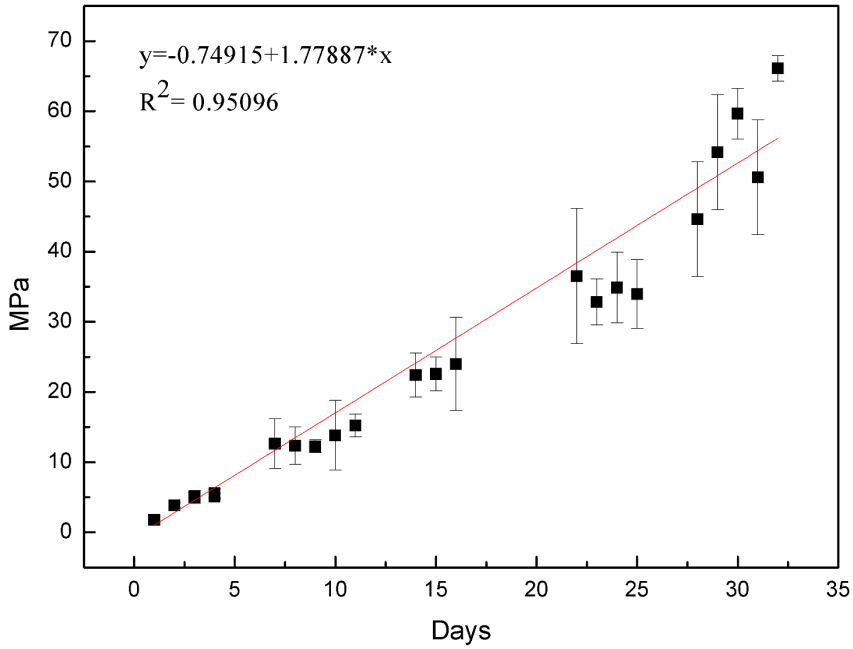

Figure 5. Compressive strength of briquettes as *fn.*, line shown as visual guide (time after forming).

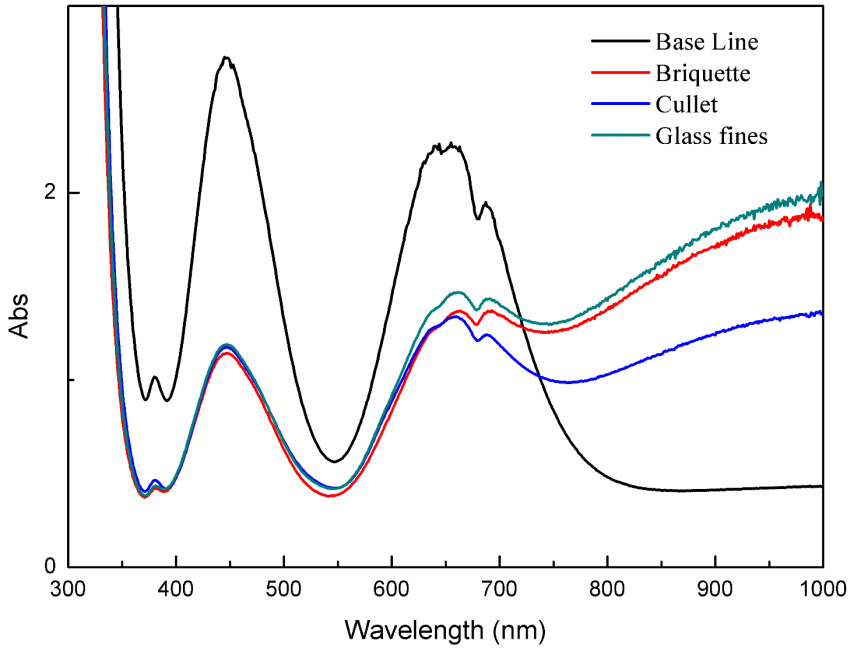

Fig.6 a) UV-Vis-Near IR absorption spectra of baseline, melted briquette, melted cullet and melted glass fines samples.

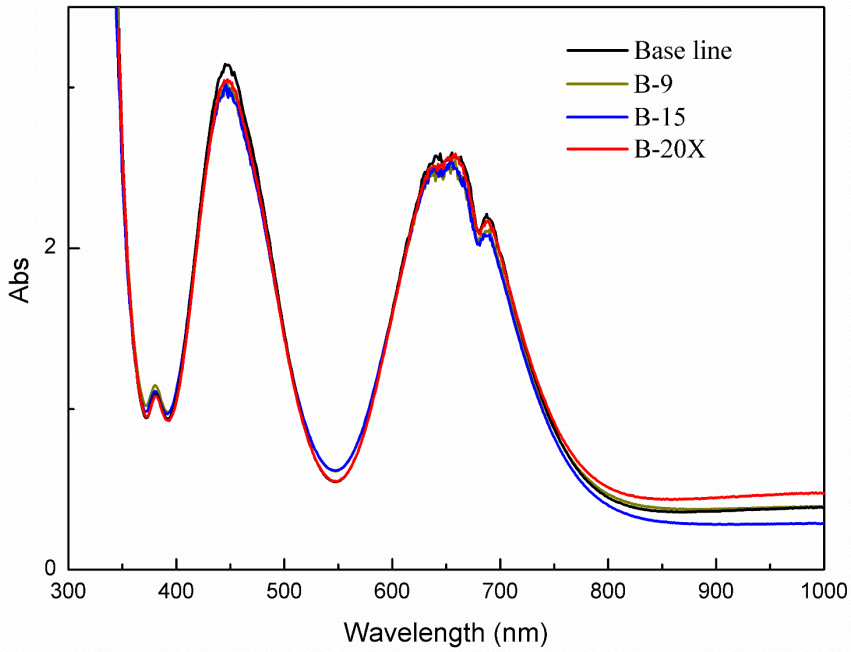

Fig.6 b) UV-Vis-Near IR absorption spectra of samples baseline, B-9, B-15 and B-20X.

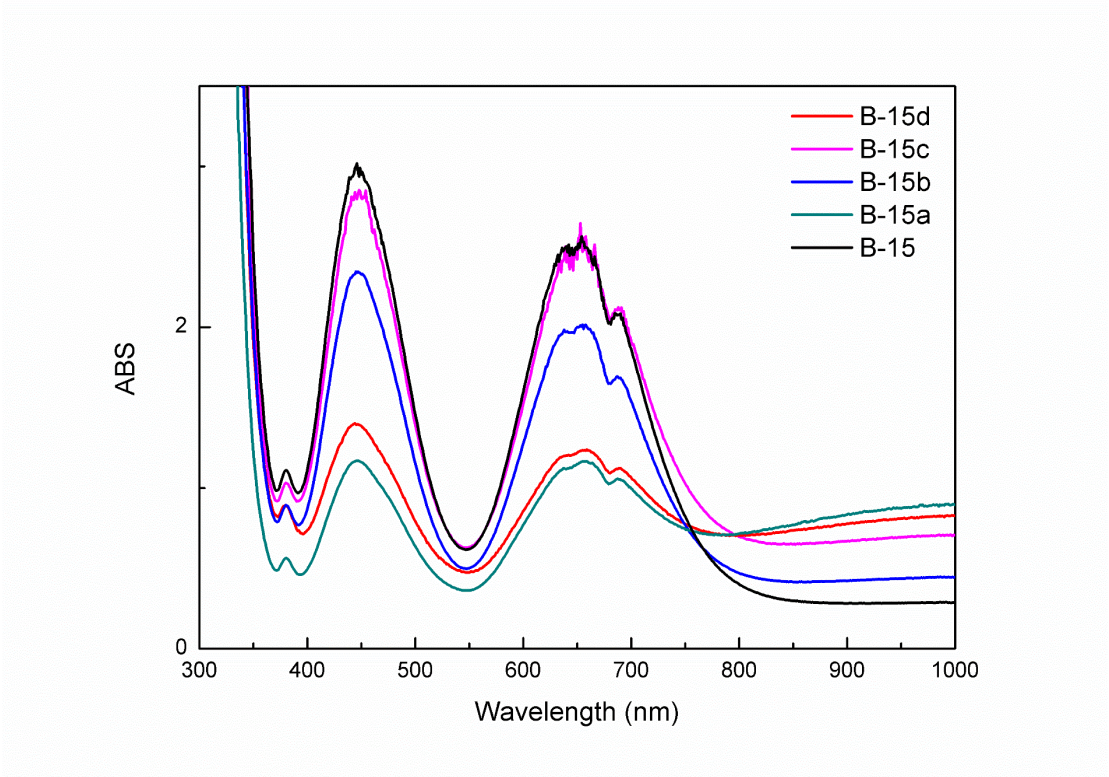

Fig.6 c) UV-Vis-Near IR absorption spectra of samples B-15, B-15a, B-15b, B-15c and B-15d.

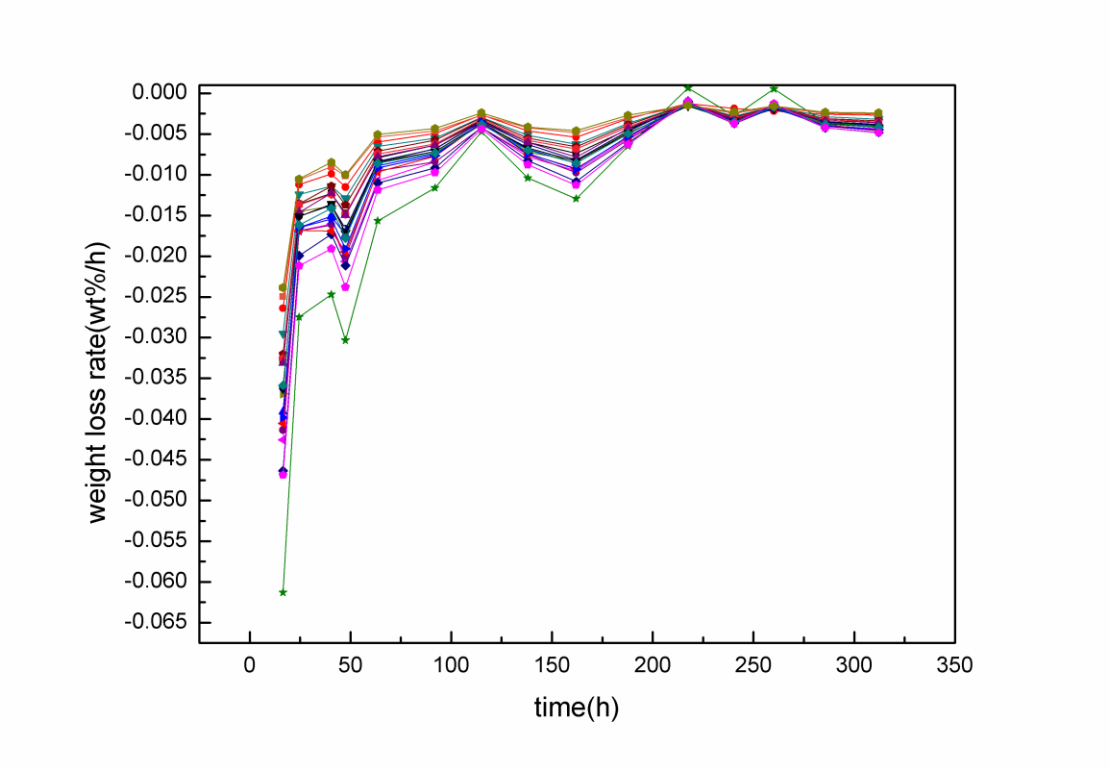

Fig.7 a) Weight loss rates for different briquettes as *fn.* (time) at 20 ^{o}C.

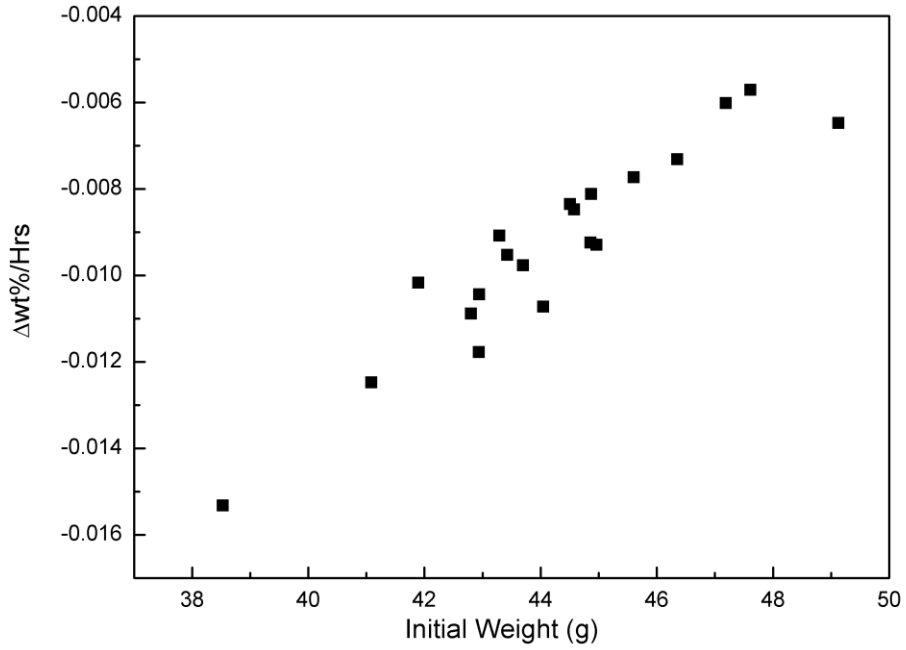

Fig.7 b) Average weight loss rate of 20 briquettes after 187 hours vs. initial weight of briquettes.

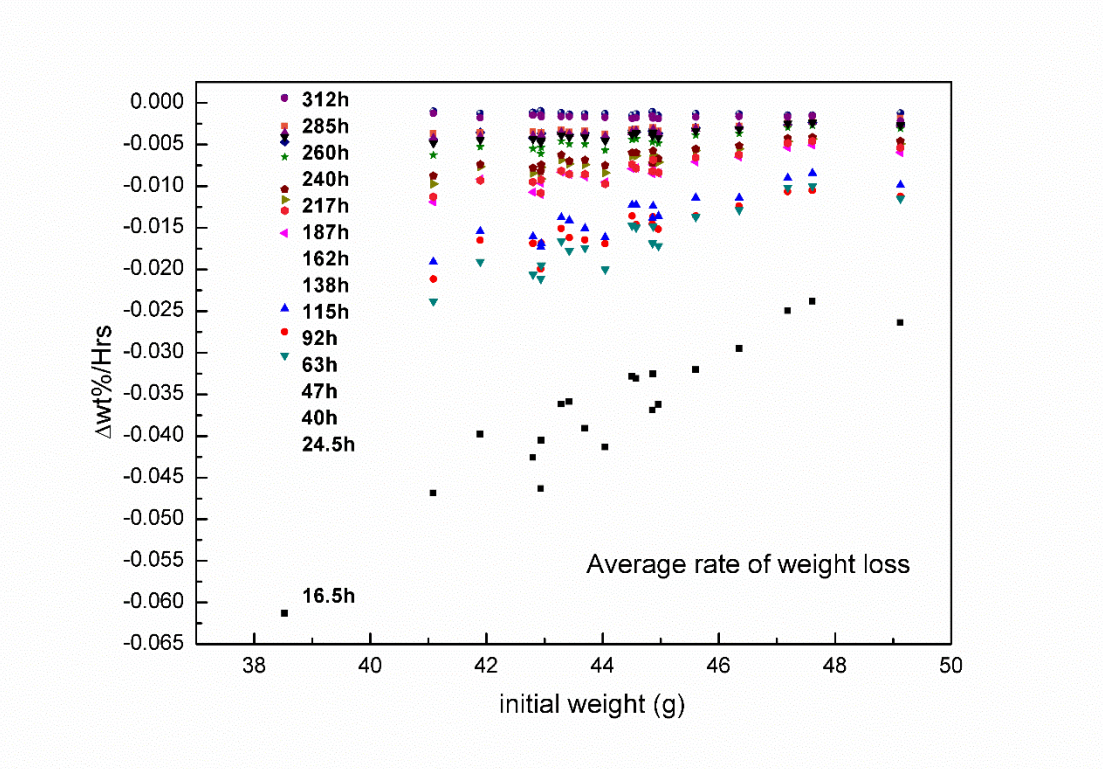

Fig.7 c) Average weight loss rate of 20 briquettes in different time vs. initial weight of briquettes.